INTEGRATED 2D 4-C OBC ANALYSIS FOR ESTIMATING HYDRATE CONCENTRATIONS, GREEN CANYON, GULF OF MEXICO

M.V. DeANGELO, D.C. SAVA, B.A. HARDAGE and P.E. MURRAY

Bureau of Economic Geology, John A. and Katherine G. Jackson School of Geosciences, The University of Texas at Austin, Austin, Texas 78713-8924, U.S.A.
mike.deangelo@beg.utexas.edu

(Received November 12, 2009; revised version accepted May 1, 2010)

ABSTRACT

DeAngelo, M.V., Sava, D.C., Hardage, B.A. and Murray, P.E., 2010. Integrated 2D 4-C OBC analysis for estimating hydrate concentrations, Green Canyon, Gulf of Mexico. *Journal of Seismic Exploration*, 19: 263-278.

A 2D four-component ocean-bottom-cable seismic survey, originally acquired for the exploration of deeper hydrocarbon targets, was used to estimate near-seafloor hydrate concentrations in the Genesis Field, Green Canyon area of the Gulf of Mexico. The high-resolution properties of the P-P and P-SV processed as common-receiver gathers were utilized to image subtle features of near-seafloor geology. Interpretation of depth equivalent events on P-P and P-SV near-offset images constrained V_P/V_S ratios and zero-offset reflection times. These events were used as inputs to create near-seafloor (<600 m below seafloor) compressional-wave and shear-wave interval velocity models. These interval velocities were used with local resistivity logs to estimate hydrate concentration using a statistical joint inversion procedure. This joint inversion method is especially critical for estimating hydrate concentration in deep-water near-seafloor strata because of the lack of sonic log measurements across the hydrate stability zone.

KEYWORDS: hydrate, ocean-bottom-cable, deep-water, inversion, P-P, P-SV.

0963-0651/10/$5.00

INTRODUCTION

The purpose of the study was to determine what information about the near-seafloor sediment (< 600 m below seafloor) could be obtained by analysis of 2D four-component ocean-bottom-cable (2D 4-C OBC) seismic data originally acquired for the exploration of deeper targets. Seismic data were acquired in the deep water (> 500 m) Gulf of Mexico (GOM), offshore Louisiana, Green Canyon, over an area of approximately 2200 km^2. A subset of the data (Fig. 1) was used to develop methodologies to characterize seafloor properties across known gas hydrate zones (Roberts, 1995; Sassen et al., 2001, 2003). Previous work details how high-resolution P-P and P-SV images were created from 2D 4-C OBC seismic data (Backus et al., 2006) and iterative seismic raytrace analysis (DeAngelo et al., 2008) determined robust interval values of subseafloor V_P and V_S velocities across a series of Earth layers extending from the seafloor to below the base of the hydrate stability zone (BHSZ). This manuscript completes the research by detailing how a rock physics model was developed relating interval V_P and V_S velocities and resistivity log data to estimates of hydrate concentrations using a joint inversion process.

Study Site

The study used data acquired in Genesis Field in the Green Canyon area (Fig. 1), Gulf of Mexico. The site was selected based on the availability of multiple data sets. First, low-frequency (10-200 Hz) 2D 4-C OBC seismic data and high-frequency (1-10 kHz) autonomous underwater vehicle (AUV) data were acquired over the same spatial locations. Second, geotechnical reports were available describing laboratory measurements of seafloor sediment properties made on seafloor borings at Genesis Field. These measurements were critical for calibrating sediment properties to seismic attributes. Third, the seafloor across portions of the study site exhibited bright reflectivity, a demonstrated proxy to indicate a subseafloor hydrate system (Roberts et al., 1992, 2006).

Data Acquisition Parameters

The 2D 4-C OBC seismic data were acquired using sensors with receiver group intervals of 25 m and a towed airgun source 6 m below sea level fired at 50 m intervals directly over the receiver cables in the corresponding line directions. A grid of 2D data lines arranged north-south and east-west at 3.2 km line spacing were used for this study. Record lengths are 18.432 s acquired at a sampling interval of 2 ms. Source-receiver offsets recorded vary from 0 to $\pm$12000 m. For the purpose of this study, data was limited to $\pm$3000 m offsets and receiver locations in water depths of 500-1000 m.

AUV data were also used for this study. An AUV system uses inertial guidance to steer an unmanned, self-propelled vehicle along a preselected path at a height of about 50 m above the seafloor. Navigation accuracy is precise, with deviations from a preprogrammed trajectory being on the order of 1 or 2 m over a traverse of one lease block (4800 m). AUV data consist of side-scan sonar, multibeam bathymetry, and chirp-sonar. Chirp-sonar data were important in this study because they provided high-resolution P-P images of seafloor strata to subseafloor depths of approximately 50 m. Approximately 80 km of AUV data were acquired for this study. The AUV data acquisition locations are shown on Fig. 1. These multicomponent and multi-frequency data form the critical remote measurements that were analyzed to determine the advantages of combining P-wave and S-wave data to evaluate deepwater hydrate systems.

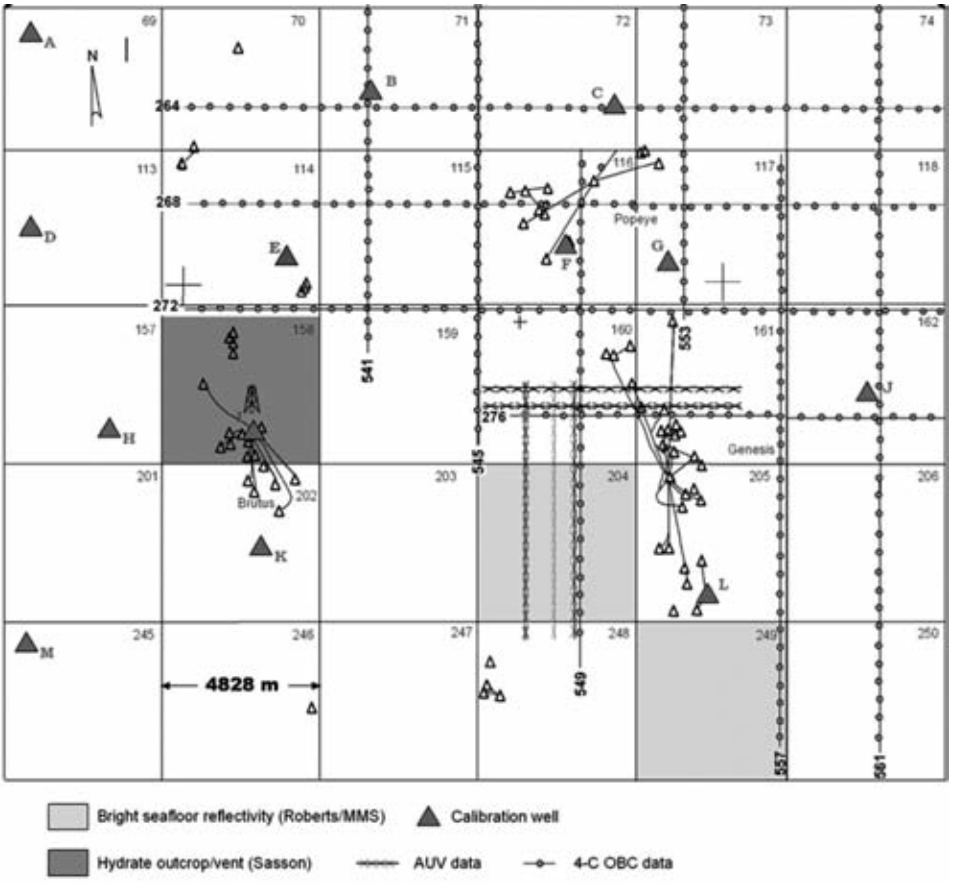

Fig. 1. Location map of 2D 4-C OBC seismic data used in the project. We limited our data to ±3000 m offsets and receiver locations in water depths of 500-1000 m. Approximately 200 km of OBC data were processed in this study. AUV = autonomous underwater vehicle.

METHODS

Data Processing

The 2D 4-C OBC data were reprocessed in the common-receiver gather (CRG) domain to create images of the near-seafloor environment with better bandwidth and higher resolution than conventional common-midpoint processing techniques. Hydrophone (P), vertical geophone (Z) and radial/inline geophone (X) data were combined to recover P-P and P-SV reflectivity. Prior to estimating reflectivity, it was necessary to define a calibration procedure to relate the output of the pressure sensors (P) to the velocity sensors (X and Z). This calibration was accomplished by identifying pure upgoing waves on both sets of sensors (refracted arrivals and wide-angle reflections) which were then used to derive a frequency-dependent cross-equalization filter. A single calibration filter for all X sensors, and a corresponding filter were derived for all Z sensors using a least-mean-square error approach from a representative receiver location. Once calibrated, it is possible to combine P and Z to separate upgoing from downgoing P-waves according to the procedure of Schneider and Backus (1964).

These estimated downgoing P wavefields were then deconvolved from upgoing (via frequency domain division) to create band-limited estimates of P-P reflectivity. To create P-SV reflectivity estimates, the downgoing P wavefields from the previous step were deconvolved from both the P and X components. Using a cross-equalization approach, P-P waves were then removed from the deconvolved X-component to isolate converted P-SV reflection events. Details of this approach are similar to that in Backus et al. (2006), except this research applied the cross-equalization step after deconvolution as noted in DeAngelo et al. (2008).

The resulting common-receiver gather estimates of P-P and P-SV reflectivity were then offset limited and summed to common-receiver P-P and P-SV stacks using 0-200 m and 200-400 m offsets, respectively. Lowcut filters (5 Hz) and weighted-trace mixing was used in some stacks to aid interpretation and enhance visual quality.

A key finding of this study was demonstrating low-frequency (10-200 Hz) converted-shear (P-SV) data extracted from 2D 4-C OBC seismic data provide amazing vertical resolution (< 1 m) of deepwater, near-seafloor geology. This is shown by comparing air-gun-generated P-SV images with high-frequency (1-10 kHz) compressional-wave (P-P) images acquired with AUV technology over the same spatial locations, as shown in Fig. 2.

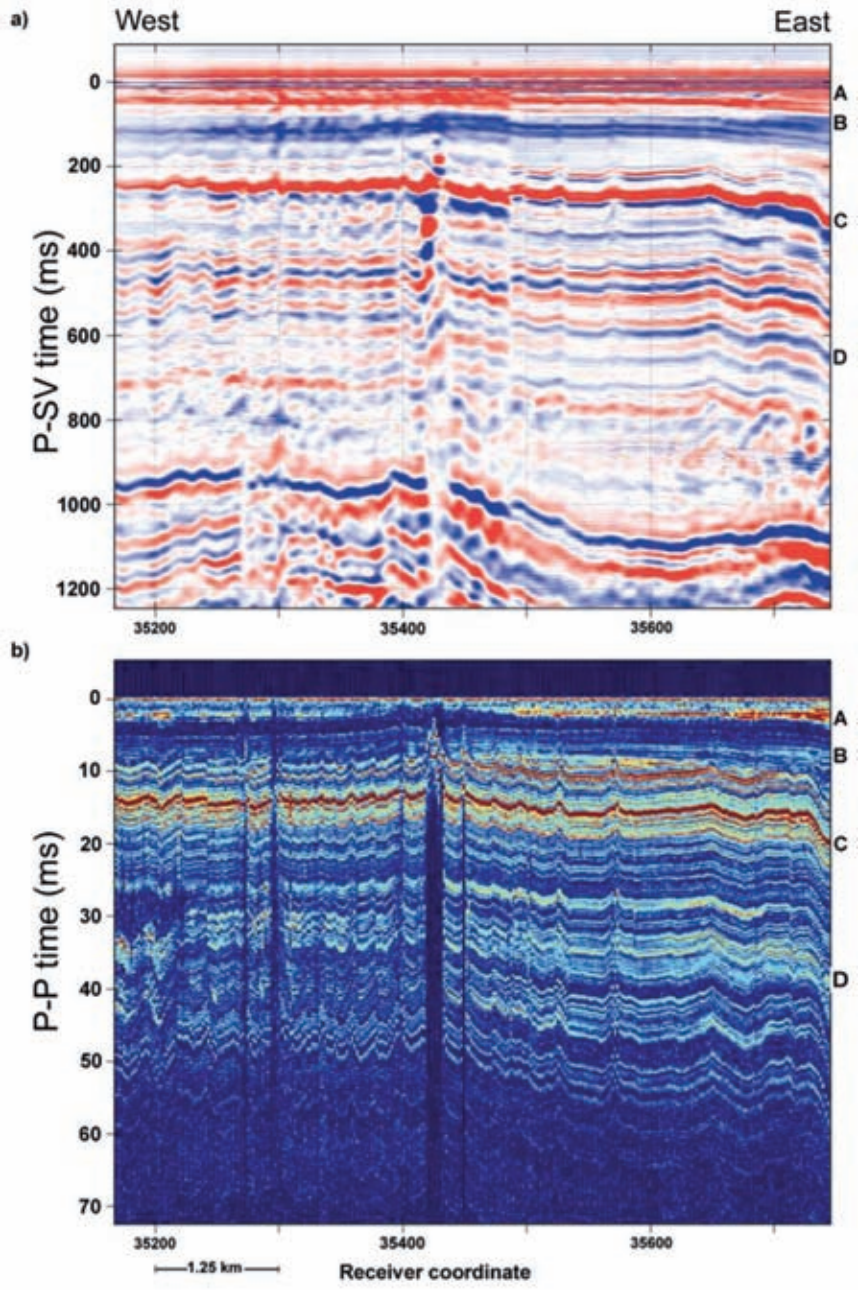

Fig. 2. Comparison of (a) OBC P-SV image and (b) AUV P-P image along OBC line 276, Genesis Field area. These images extend across portions of Blocks GC160 and GC161 (Fig. 1). Interpreted depth-equivalent horizons A, B, C, and D are labeled on the right margin. All images are shown relative to a flattened seafloor.

It is important to note each OBC P-SV image can resolve an interfaces that are within 1 m of the seafloor, whereas, AUV P-P data along several lines do not image this horizon. Low-frequency OBC P-SV data can resolve some near-seafloor geologic features better than do high-frequency AUV P-P data. This is due to the low values of V_S velocity in the shallowest seafloor strata (which were measured as low as 25 m/s) which yield very short wavelengths to enable this resolution. It is also important to note the high V_P/V_S ratios yielded from this analysis. In the shallowest interpreted layers, these ratios can approach 60 (Backus et al., 2006).

The image comparisons illustrated on Fig. 2 are typical of the AUV P-P and OBC P-SV image registrations along all of the AUV lines that were studied in this project. Except for small areas local to some expulsion features, depth-equivalent P-P and P-SV horizons that were interpreted for the AUV P-P and OBC P-SV lines established the following principles of deepwater, near-seafloor geology across our Green Canyon project area:

- The base of the hemipelagic layer is the horizon labeled C. The thickness of this layer ranges from 6-20 ms of P-P image time along the AUV lines that were available for analysis, which positions the base of the interval at subseafloor depths of 4-14 m across the project area.

- In P-SV image space, the base of the hemipelagic layer is commonly between 200-220 ms.

- A P-P image time of 30 ms, which is close to the deepest good-quality reflection seen on most AUV lines, is depth-equivalent to a P-SV image time that is in the range of 400 ms [$\pm$50 ms].

These principles apply to AUV data and OBC data acquired at Genesis Field (Fig. 1).

Interpretation

The objective of interpretations of P-P and P-SV images along each OBC line was to define which subseafloor P-SV reflection events were depth-equivalent to selected P-P reflections existing across this same subseafloor depth interval and make direct estimates of V_P/V_S ratios within the interpreted intervals. Interpretations were limited to reflection events estimated to occur within the gas hydrate stability zone. The near-seafloor section contained few geometric features such as structural or stratigraphic terminations that could be used to constrain the interpretation. An attempt to register fault surfaces was made; however, the shallow faults were sufficiently steep to make correlation ambiguous.

Seismic character variations (amplitude, phase, and frequency) between the P-P and P-SV data presented additional obstacles for the interpreter to overcome when correlating between the two seismic modes (Fig. 3). Determining reliable velocity estimates within the shallow subseafloor layers required a rigorous numerical analysis to determine if each pair of tentatively interpreted P-P and P-SV reflections were truly depth-equivalent, or whether alternate events needed to be selected to establish robust depth equivalency.

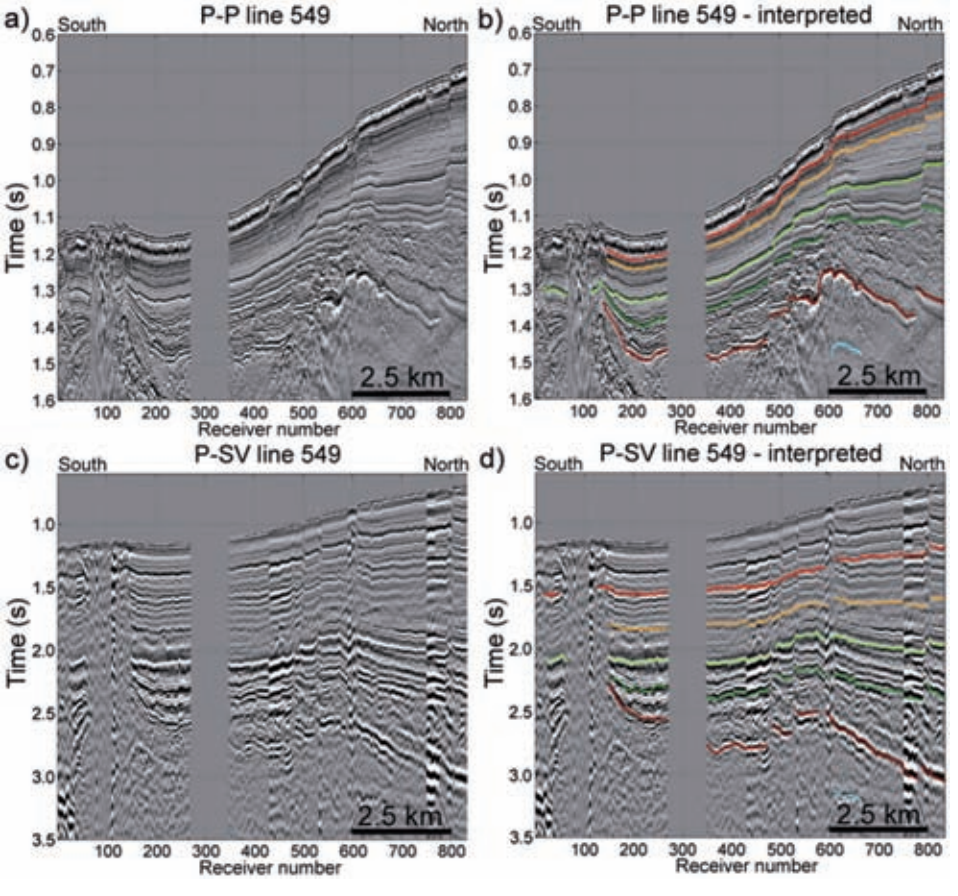

Fig. 3. Interpretation of OBC line 549, (a) P-P image created from limited-offset stacks of receiver gathers, (b) interpreted P-P image, (c) P-SV image created from limited-offset stacks of receiver gathers, and (d) P-SV image with depth-equivalent interpretations.

Raytracing

The arrival times of reflections were numerically estimated using a simple 1D raytracing approach to perform velocity analysis on common-receiver gathers as outlined in DeAngelo et al. (2008). To create interval velocity models from stacked images and common-receiver gather (CRG) data, the following steps were implemented:

1. Interpreted depth-equivalent reflection events on the P-P and P-S images.

2. Use the T_{PP} and T_{PS} times to constrain the V_P/V_S ratios and the zero-offset reflection times at the corresponding CRG locations.

3. Use 1D ray-tracing to create a model of V_P, V_S, and layer thickness that aligns predicted reflection travel times with corresponding events in the CRGs.

4. Repeat for each successively deeper layer at a given CRG location.

5. Interpolate velocity models between velocity analysis locations.

Although the water layer has been removed from the CRG in the reduced-time domain, it must still be included in the ray-trace calculation and then subtracted from the total travel times to properly align predicted events with interpreted data.

Velocity analysis was performed at every 10 to 20 common-receiver gathers, and interpolated the velocity models to create velocity profiles of V_P and V_S as shown in Fig. 4. At each subseafloor depth coordinate, we modeled the joint theoretical relations between hydrate concentration c_{gh} (our model parameter), resistivity R and seismic propagation velocities (V_P and V_S) of subseafloor strata (the observed parameters) using the Monte Carlo procedure previously described to create posterior probability distributions of gas hydrate concentration at each spatial location analyzed.

Joint Inversion of Resistivity and Velocity

Gas hydrates increase both the elastic moduli and the electrical resistivity of the sediments in which they occur. However, the relation between hydrate concentration and resistivity of strata containing hydrates is non-unique and uncertain. This is also true of the relationship between hydrate concentration and velocity. Some of these sources of uncertainty are limited availability of data, accuracy in defining mineral fractions in the host sediment, porosity, physical

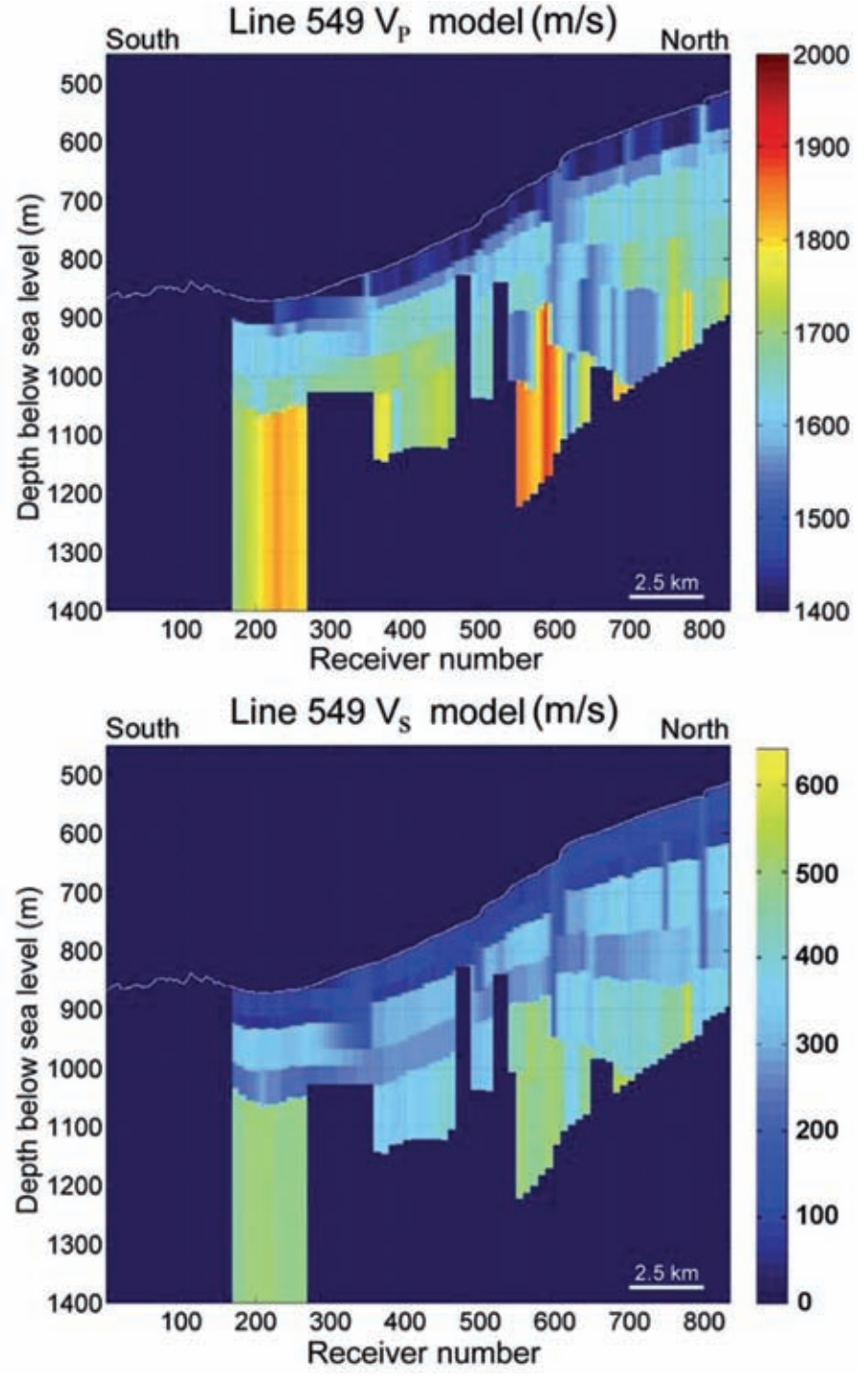

Fig. 4. Interpolated interval V_P and V_S models across OBC line 549 (compare with Fig. 3).

distribution of hydrate within the host sediment, unaccounted spatial variability of rock properties, and inadequate understanding of other physical conditions and processes associated with hydrate systems. Predictions of gas hydrate distribution can be better restrained by performing a joint inversion of the electrical resistivity and seismic information.

The joint inversion technique is a Bayesian approach, combining rock-physics elastic theories (Helgerud et. al, 1999; Sava and Hardage, 2006) and empirical relations for electrical resistivity (Archie, 1942) as modified for clay-bearing sediments proposed by Schlumberger Wireline and Testing (1989). This study uses stochastic simulations to account for the natural variability of the petrophysical parameters involved in the inversion. This approach to inverse problems was proposed by Tarantola (1987), which allows the estimation of the hydrate concentration and also provides a measure of the uncertainty associated with the predictions.

Each parameter in the rock-physics elastic model and the empirical Archie Equation is expressed as a probability density function (PDF). The PDFs used in this joint inversion are either Gaussian distributions or uniform distributions. Gaussian distributions are used when the expected value for the model parameter is known. A uniform distribution is used when the value of a parameter is unknown but the range of variability for the parameter can be defined.

First, forward modeling was utilized to derive the joint theoretical relation between the hydrate concentration with both electrical resistivity and seismic velocities. Both seismic velocities and the electrical resistivity depend on porosity of the sediment, hydrate concentration, and clay content. These parameters are referred as common parameters, since both electrical resistivity model (modified Archie Equation) and the elastic rock physics models depend on them. A Monte Carlo procedure was used to draw values from the PDFs of these common parameters and from the PDFs of each petrophysical parameter used in the forward models of a hydrate system. Then, the actual values from electrical resistivity logs and from seismic velocities were used to estimate the hydrate concentration in situ. Therefore, the outcome of the joint inversion is the posterior probability distribution function of gas hydrate concentration.

At each subseafloor depth coordinate, the joint theoretical relations between hydrate concentration c_{gh} (the model parameter we need to calculate), the resistivity R, and seismic propagation velocity (both V_P and V_S) of subseafloor strata (which represent the observed parameters) were modeled. A Monte Carlo procedure was used to draw values for common parameters, hydrate concentration, porosity and volume of clay from their associated PDFs and then compute the corresponding velocity and resistivity values using Monte Carlo draws from the PDFs for each of the model parameters that are required for calculating hydrate concentration.

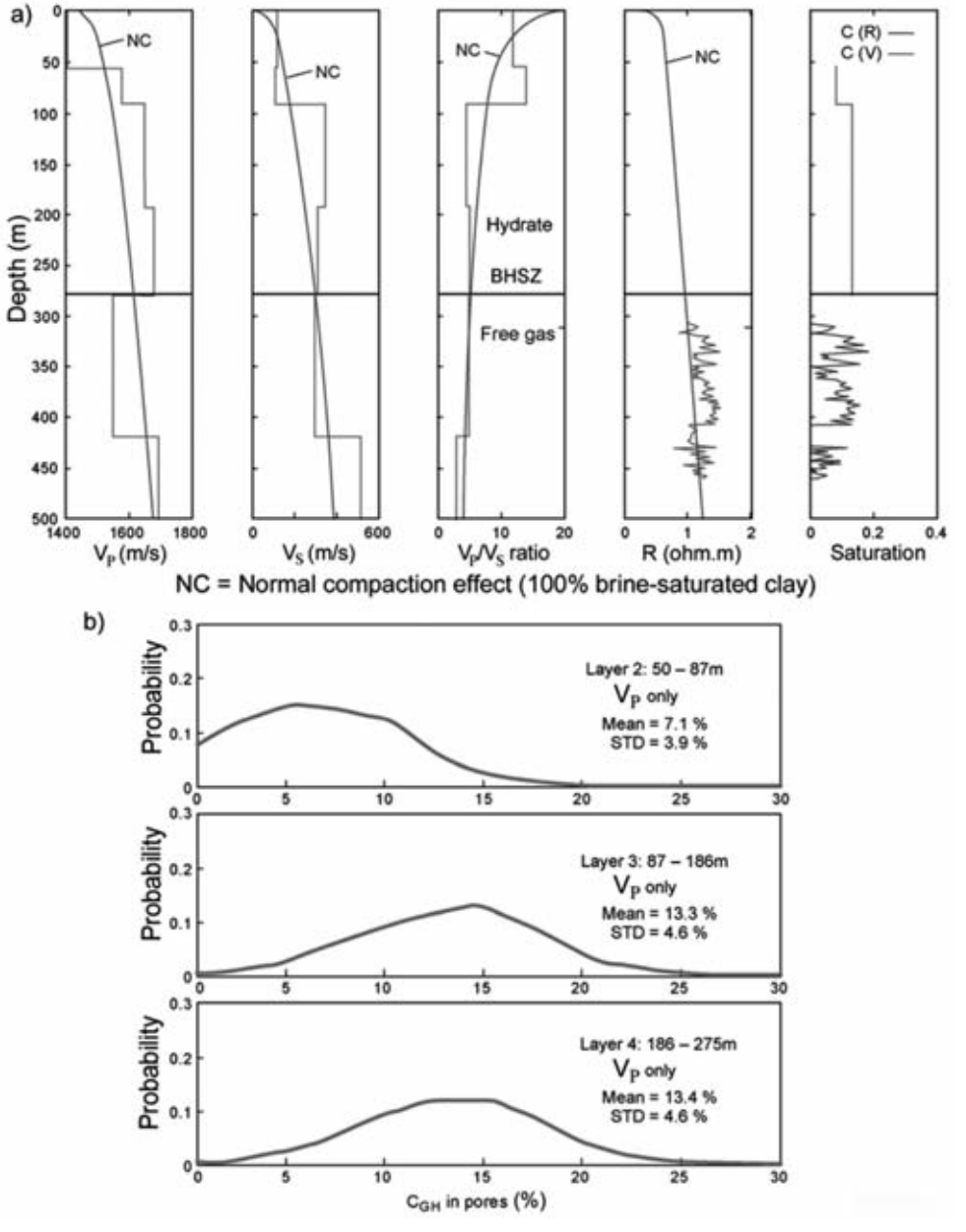

Fig. 5. (a) Seismic-based V_P and V_S interval velocities, resistivity log, and their respective estimates of hydrate concentration at Well C (Fig. 1). The BHSZ boundary is defined as the top of the layer where V_P velocity exhibits a reversal in magnitude. The increase in resistivity below the BHSZ boundary is caused by free gas. (b) Only V_P velocity can be used for inversion. Inversion results are shown for velocity Layers 2, 3, and 4.

The joint inversions (Ex. Fig. 5) established the fundamental calibration points that allowed seismic interval velocities determined along each OBC line to be inverted into reliable estimates of hydrate concentration that were far from any calibration well. The velocity inversion is simplified by using an average V_P velocity across each velocity-layer interval. As a result, the velocity-dependent hydrate concentration shown on the right panel of the figure is a constant value across each velocity layer. It was concluded this simplification was sufficient for a "big picture" view of hydrate concentration.

Relationships between V_P velocity and hydrate concentration developed at calibration wells were applied to the V_P velocity layer models constructed along each OBC line. The inversion results for the velocity layering along OBC line 549 are displayed as Fig. 6. Along the southern half of the line, the BHSZ boundary was defined as the onset of a reversal in V_P magnitude. Along the northern half of each line, the BHSZ boundary was defined by the water-depth-based thermal constraint for 90% methane hydrate published by Milkov and Sassen (2001).

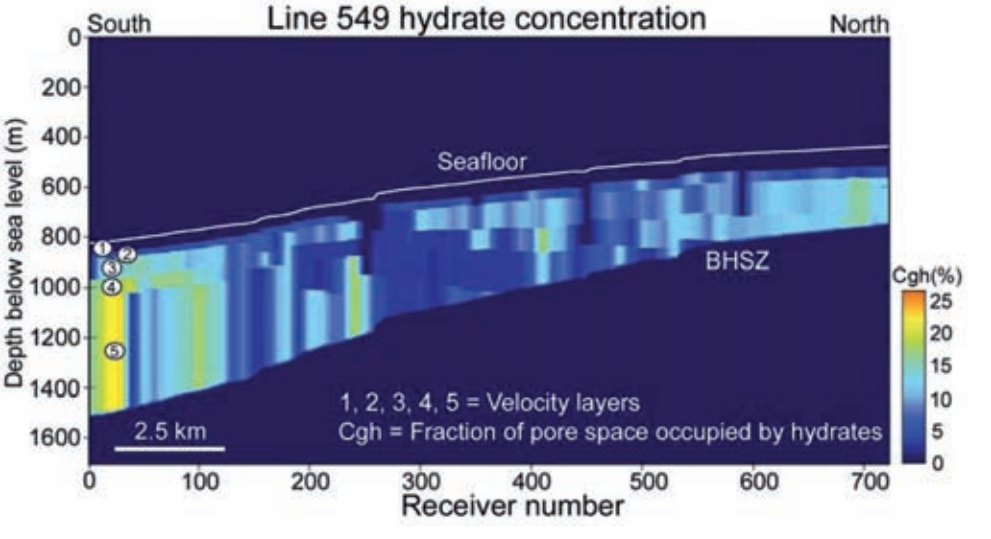

Fig. 6. Hydrate concentrations estimated along OBC line 549. Hydrate concentration was not estimated for Layer 1 because no log data were available to confirm the trend of the normal compaction curves across this shallowest interval immediately below the seafloor. At the south end of the line, the BHSZ boundary is defined by a reversal of V_P velocity. At the north end, the Milkov and Sassen (2001) thermal constraint for 90% methane hydrate is used to define the BHSZ.

Because Layer 1 immediately below the seafloor had no log data available across this shallowest layer we assigned a constant, near-zero hydrate concentration to Layer 1 and focused our hydrate estimation on velocity Layer 2 and deeper layers that extend down to the BHSZ horizon. Velocity analyses did not indicate a velocity magnitude in Layer 1 anywhere across the OBC line that would infer hydrate was present in this shallowest layer. Calculated hydrate concentrations exhibit considerable lateral spatial variation within each velocity layer and even greater vertical variability from layer to layer. The hydrate concentrations were local, including limited areas where hydrate occupied a little more than 30% of the pore space of the host sediment.

To determine the amount of in situ hydrate existing within the interval extending from the seafloor to the BHSZ boundary, the seismic-based hydrate concentrations (expressed as the fraction of occupied pore space) was multiplied

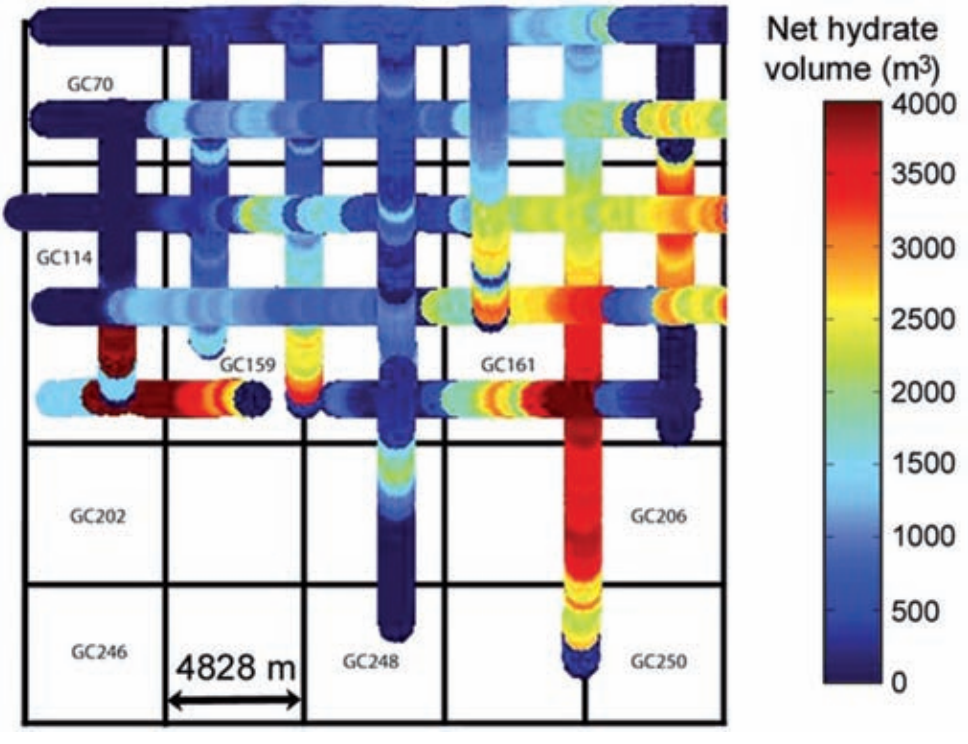

Fig. 7. Amount of in situ hydrate across study area. The values plotted on this map are the product: (hydrate concentration) × (layer porosity) × (layer thickness) × (250 m). The 250 m factor is the distance between adjacent velocity analysis points where V_P velocities are calculated. The color bar defines the amount of in situ hydrate below a 1 m × 250 m strip centered on the sequence of seafloor receiver stations where velocity analyses were done.

by each layer thickness and layer porosity and summed these products to create an estimate of total in situ hydrate. A map of in situ hydrate across the study area is shown as Fig. 7. Seismic-based quantification of in situ hydrate indicates the largest accumulation of hydrate exists in Green Canyon Blocks GC161, GC162 in the Genesis Field, and GC158 west of the Genesis Field (Fig. 7). At some locations across this trend, the amount of in situ hydrate is estimated to be as much as 4000 m^3 beneath 1 m $\times$ 250 m rectangular strips centered on receiver stations where V_P interval velocities were determined for estimating hydrate concentration.

CONCLUSIONS

Several new technologies were developed to estimate hydrate concentrations in strata spanned by the hydrate stability zone that extends across the deepwater area of Green Canyon. Key technology developments were:

1. Calibration of hydrophone and geophone sensor responses to create optimal estimates of downgoing and upgoing wavefields when adding and subtracting hydrophone and geophone data.

2. A new strategy for processing 2D 4-C OBC seismic data that produces high-resolution P-P and P-SV images of near-seafloor geology.

3. A new raytrace procedure that creates a model of subseafloor layering of V_P and V_S velocities at selected seafloor-receiver stations.

4. Rock physics models that relate seismic velocities to hydrate concentration for four different sediment-hydrate morphologies.

5. The use of probability distribution functions to describe all variables that are used to estimate hydrate concentration.

6. The use of joint inversion of resistivity and velocity to constrain our predictions of hydrate concentration to a range of most-probable expectation.

These techniques established that hydrate is pervasive across the Genesis Field, Green Canyon area. The hydrate concentration was generally less than 15% of the available pore space. In a few local areas concentrations increased to more than 30% of the pore space of the host sediment. In addition, it was determined that a free-gas layer immediately under lays the base of the hydrate stability zone across the study area. This free-gas zone is revealed by a reduction in V_P velocity determined by using a high-resolution raytrace modeling technique. The amount of free gas in this zone was not estimated, but it is

expected that the zone has a gas saturation zone of only a few percentage points. Domenico (1976) has demonstrated that a small amount of free gas can produce a significant reduction in V_P velocity. This free-gas zone was not easily distinguished from a hydrate-bearing zone when examining resistivity logs available across the area. The observed increase in log resistivity related to free gas can be confused with a resistivity increase caused by hydrate. Thus interpreting the thickness of the hydrate stability zone from resistivity logs alone can lead to an overestimation of the thickness of stable hydrate and of the amount of hydrate that is present.

Additional technologies should be considered in future hydrate studies. Foremost among the applications that should be tried would be an inversion of the P-P and P-SV seismic data to create a trace-by-trace, datapoint-by-datapoint estimation of seismic impedance rather than relying on the averaged, layered velocities that we used. The higher spatial resolution of velocity behavior provided by inversion of P-P and P-SV traces should provide more detail about the internal fabric of the hydrate systems than what we have achieved with our larger-scale, interval-velocity approach.

The seismic data processing strategy should be adjusted so that water-column multiples are removed from the data. Because water depths ranged from 500-1000 m across the area, water-column multiples begin arriving at delay times ranging from 670-1330 ms (500-1000 m water depth), assuming a propagation velocity of 1500 m/s in seawater. These delay times placed the multiples near or immediately below the BHSZ in P-P image space which allowed the use simple data processing strategies that involved no demultiple operations. However, water-column multiples did contaminate our P-SV data within the hydrate stability zone and sometimes even contaminated the P-P data near the base of the hydrate stability zone. These multiples sometimes made it difficult to interpret velocity layers near the BHSZ boundary where it is important to know if a velocity inversion is present. If similar deepwater hydrate studies are done in the future, it will be wise to remove the water-column multiples on all OBC sensor data.

ACKNOWLEDGMENTS

This article was prepared with the support of the U.S. Department of Energy (DOE) under Contract No. DE-FC26-05NT42667. However, any opinions, findings, conclusions, or recommendations expressed herein are those of the authors and do not necessarily reflect the views of the DOE. Support for this work was provided in part by the John A. and Katherine G. Jackson School of Geosciences and the Geology Foundation at The University of Texas at Austin. As an industry partner, WesternGeco provided the 2D 4-C OBC data. Landmark Graphics Corporation provided software for the basic 2D seismic

interpretation via the Landmark University Grant Program. The illustrations were prepared with the assistance of Joel L. Lardon, Manager of Media Services. Publication was authorized by the Director, Bureau of Economic Geology, The University of Texas at Austin.

REFERENCES

Archie, G.E., 1942. The electric resistivity log as an aid in determining some reservoir characteristics. Petrol. Transact. Am. Inst. Mining, Metallur. Petrol. Engin., 146: 54-62.

Backus, M.M., Murray, P.E., Hardage, B.A. and Graebner, J., 2006. High-resolution multicomponent seismic imaging of deepwater gas-hydrate systems. The Leading Edge, 25: 578-596.

DeAngelo, M.V., Murray, P.E., Hardage, B.A. and Remington, R.L., 2008. Integrated 2D 4-C OBC velocity analysis of near-seafloor sediments, Green Canyon, Gulf of Mexico. Geophysics, 73: B109-B115.

Domenico, S.N., 1976. Effect of brine-gas mixture on velocity in an unconsolidated sand reservoir. Geophysics, 41: 882-894.

Helgerud, M.B., Dvorkin, J., Nur, A., Sakai, A. and Collet, T., 1999. Elastic-wave velocity in marine sediments with gas hydrates: Effective medium modeling. Geophys. Res. Lett., 26: 2021-2024.

Milkov, A.V. and Sassen, R., 2001. Estimate of gas hydrate resource, northwestern Gulf of Mexico continental slope. Mar. Geol., 179: 71-83.

Roberts, H.H., 1995. High-resolution surficial geology of the Louisiana middle-to-upper continental slope. Gulf Coast Assoc. Geol. Soc. Transact., 45: 503-508.

Roberts, H.H., Hardage, B.A., Shedd, W.W. and Hunt Jr., J., 2006. Seafloor reflectivity - An important seismic property for interpreting fluid/gas expulsion geology and the presence of gas hydrate. The Leading Edge, 25: 620-628.

Roberts, H.H., Cook, D.J. and Sheedlo, M.K., 1992. Hydrocarbon seeps of the Louisiana continental slope: Seismic amplitude signature and sea floor response. Gulf Coast Assoc. Geol. Soc. Transact., 42: 349-362.

Sassen, R., Losh, S.L., Cathles III, L., Roberts, H.H., Whelan, J.K., Milkov, A.V., Sweet, S.T. and DeFreitas, D.A., 2001. Massive vein-filling gas hydrate: relation to ongoing gas migration from the deep subsurface of the Gulf of Mexico. Mar. Petrol. Geol., 18: 551-560.

Sassen, R., Milkov, A.V., Ozgul, E., Roberts, H.H., Hunt, J.L., Beeunas, M.A., Chanton, J.P., DeFreitas, D.A. and Sweet, S.T., 2003. Gas venting and subsurface charge in the Green Canyon area, Gulf of Mexico continental slope: evidence of a deep bacterial methane source? Organic Geochem., 34: 1455-1464.

Sava, D.C. and Hardage, B.A., 2006. Rock physics characterization of hydrate-bearing deepwater sediments. The Leading Edge, 25: 616-619.

Schlumberger Wireline Services, 1989. Log interpretation principles/applications. Schlumberger Educational Serv., Houston, TX.

Schneider, W.A. and Backus, M.M., 1964. Ocean-bottom seismic measurements off the California coast. J. Geophys. Res., 69: 1135-1143.

Tarantola, A., 1987. Inverse Problem Theory. Elsevier Science Publishers, Amsterdam.